Second IEEE Conference on Control Applications, September 13 - 16, 1993 Vancouver, B.C.

Impedance Control Without Using Velocity Measurements

Mile Erlic and W.-S. Lu

Department of Electrical and Computer Engineering, University of Victoria
Victoria, British Columbia, Canada V8W 3P6

Abstract — An impedance controller has been realized using an end-effector force/torque sensor and joint displacement sensors only. Joint velocities are obtained with a reduced order nonlinear velocity observer. The system dynamics exhibit locally asymptotically stable end-effector Cartesian position, velocity and force tracking. The observer plus impedance controller has been simulated resulting in strong correlation between theory and simulation.

1. INTRODUCTION

The two techniques of primary importance in manipulator force control are impedance control [1], [2], [3] and hybrid position/force control [4]. In the former a mechanical impedance is specified for the Cartesian motion of the manipulator with a model based controller which requires position, velocity and contact force feedback. In the latter, the force and position control problems are decoupled and independent controllers are simultaneously implemented for position and force control respectively. Both of these controllers require position, velocity and force feedback.

Often, manipulators are absent of velocity sensors for a variety of reasons including procurement expense and system integration costs. Yet, a velocity estimate is required to implement the impedance and position/force controllers. Velocity estimates can be obtained by numerically differentiating position signals. However, even low levels of measurement noise in the position signal may render the velocity estimate of no use in control. An alternative to numerical differentiation is the use of a velocity observer. This is preferred since observers use integrators in their implementation; as such, they mitigate the effects of noise which may be present in the position measurement.

Several manipulator velocity observers have been suggested for unconstrained motions. In [5] and [6] full order velocity observers were presented which exhibit second order dynamics. In [7] a reduced-order observer was suggested which has first order dynamics. In this paper, the observer presented in [7] has been adopted for constrained motions.

The velocity estimate provided by the proposed observer and is used by an impedance controller. The design of the observer plus impedance controller is based on Lyapunov stability analysis. The analysis shows that the observer error dynamics as well as the trajectory tracking error dynamics tend to zero asymptotically as long as the initial tracking and observation errors belong to a predefined region of attraction. Contact forces also converge to desired values.

2. NOTATION AND PRELIMINARIES

The dynamic equation of a constrained n degree-of-freedom manipulator operating in m-dimensional space is given by

$$H(q)\ddot{q} + C(q,\dot{q})\dot{q} + F\dot{q} + g(q) = \tau - J^T(q)F_{ext} \tag{1}$$

where $q \in \Re^n$ is the joint displacement vector, $\tau \in \Re^n$ is the vector of joint torques, $g(q) \in \Re^n$ represents the gravitational torques, $H(q) = I_r(q) + I_m \in \Re^{n \times n}$ is a matrix consisting of the rigid link inertia matrix $I_r(q)$ and motor and gear inertia matrix I_m, $C(q,\dot{q})\dot{q} \in \Re^n$ is the vector of Coriolis and centripetal torques, $F = K_\omega + V \in \Re^{n \times n}$ is a diagonal matrix consisting of the back *emf* coefficient matrix K_ω and the viscous friction coefficient matrix V. The vector of external forces acting at the end-effector is denoted by $F_{ext} \in \Re^m$. This force is distributed among the joints by means of the mapping $\tau_{ext} = J^T(q)F_{ext}$, where $J(q) \in \Re^{m \times n}$ is the Jacobian matrix.

The relationships between the manipulator's joint space coordinates and its Cartesian end-effector coordinates is summarized as follows:

$$x = \mathrm{kin}(q) \tag{2a}$$
$$\dot{x} = J(q)\dot{q} \tag{2b}$$
$$\ddot{x} = J(q)\ddot{q} + \dot{J}(q,\dot{q})\dot{q} \tag{2c}$$

where $x \in \Re^{6 \times 1}$ is a vector representing end-effector position and orientation. Assuming the inverse kinematic relationships exist, we can write

$$q = \mathrm{invkin}(x) \tag{3a}$$
$$\dot{q} = J^{-1}(q)\dot{x} \tag{3b}$$
$$\ddot{q} = J^{-1}(q)\left[\ddot{x} - \dot{J}(q,\dot{q})J^{-1}(q)\dot{x}\right] \tag{3c}$$

A nonlinear change of coordinates using (3) can transform the manipulator dynamic equation (1) from joint coordinates to end-effector Cartesian coordinates, i.e.

$$H_x(q)\ddot{x} + C_x(q,\dot{q})\dot{x} + F_x(q)\dot{x} + g_x(q) = J^{-T}\tau - F_{ext} \tag{4}$$

where

$$H_x(q) = J^{-T}H(q)J^{-1}$$
$$C_x(q,\dot{q}) = J^{-T}\left[C(q,\dot{q}) - H(q)J^{-1}\dot{J}\right]J^{-1}$$
$$F_x(q) = J^{-T}FJ^{-1}$$
$$g_x(q) = J^{-T}g(q)$$

Here, $J(q)$ full rank has been assumed which implies that the manipulator does not lose any motion degrees of freedom due to singular joint configurations.

Several properties of the manipulator dynamic are summarized presently. These are useful in controller stability analysis.

Property 1. The manipulator inertia matrix is positive definite, symmetric and bounded, i.e. $m_l \le \|H_x(q)\| \le m_u$, $m_l, m_u > 0$, $\forall q \in \Re^n$.

Property 2. The 2-norm of $J^{-T}C(q,J^{-1}\dot{x})J^{-1}$ is bounded by $\|J^{-T}C(q,J^{-1}\dot{x})J^{-1}\| \le m_c\|\dot{x}\|$, $m_c > 0$, $\forall q,\dot{x} \in \Re^n$.

Property 3. The matrix of Christoffel symbols, $C(q,x)$ satisfies $C(q,x)\xi = C(q,\xi)x \quad \forall q,x,\xi \in \Re^n$ where $C(q,x)$ is uniquely defined in [8].

Property 4. $\dot{H}_x(q) - 2C_x(q,\dot{q})$ is skew symmetric, i.e. $\xi^T(\dot{H}_x(q) - 2C_x(q,x))\xi = 0 \quad \forall \xi \in \Re^n$

3. THE VELOCITY OBSERVER

Another formulation of the dynamic equation (1) gives us an explicit expression for joint acceleration, i.e.

$$\dot{y} = H^{-1}(q)\left[\tau - C(q,y)y - Fy - g(q) - J^T F_{ext}\right] \tag{5}$$

where $y = \dot{q}$. This is a first order equation in y where q is assumed known, τ is the input and y is the output. The proposed observer has a structure similar to (5) and is given by

$$\dot{\hat{y}} = H^{-1}(q)\left[\tau - C(q,\hat{y})\hat{y} - F\hat{y} - g(q) - J^T F_{ext}\right] + K\tilde{y} \tag{6}$$

where $\hat{y}$ is the *observed* velocity estimate, $\tilde{y} = y - \hat{y}$ is the observer error, $K > 0$ is a diagonal gain matrix, and $(\hat{*})$ denotes the estimate of $(*)$. Furthermore, concerning the realization of (6), we note that

$$\begin{aligned}\hat{y}(t) &= \hat{y}(t-\Delta) + K\left[q(t) - q(t-\Delta)\right] \\ &+ \int_{t-\Delta}^{t}\left\{H^{-1}(q)\left[\tau - C(q,\hat{y})\hat{y} - F\hat{y} - g(q) - J^T F_{ext}\right] - K\hat{y}\right\}dt\end{aligned} \tag{7}$$

where $\hat{y}(0)$ is a reasonable guess of $\dot{q}(0)$ and Δ is the integration interval. By subtracting (6) from (5), and using Appendix A, the observation error can be expressed in Cartesian coordinates as

$$H_x(q)\ddot{\tilde{x}} = -C_x(q,\dot{q})\dot{\tilde{x}} - J^{-T}C(q,\hat{y})J^{-1}\dot{\tilde{x}} - F_x(q)\dot{\tilde{x}} - J^{-T}H(q)KJ^{-1}\dot{\tilde{x}} \tag{8}$$

where $\dot{\tilde{x}} = Jy - J\hat{y} = J\tilde{y}$. Equation (8) describes the observer error dynamics and will be invoked in the stability analysis.

The implementation of the velocity observer (7) on a digital computer will be considered presently. Let Δ be the sampling interval over which a velocity estimation is made, then discretization of (7) at $t = i\Delta$ leads to

$$\begin{aligned}\hat{y}(t) &= \hat{y}(t-\Delta) + K\left[q(t) - q(t-\Delta)\right] \\ &+ \Delta H^{-1}(q)\left[\tau - C(q,\hat{y})\hat{y} - F\hat{y} - g(q) - J^T F_{ext}\right] - \Delta K\hat{y}\end{aligned} \tag{9}$$

where i represents the time at $t = i\Delta$.

4. IMPEDANCE CONTROL WITH AN OBSERVER

The observer presented in Section 3 can be combined with an impedance controller to give locally asymptotically stable tracking errors. The combined system will now be presented and stability analysis will prove trajectory, force and observer error convergence.

A. The Impedance Controller

The proposed impedance controller is given by

$$\begin{aligned}\tau &= J^T F_c \\ F_c &= F_{ext} + H_x\ddot{x}_v + C_x(q,\hat{y})\dot{x}_v + F_x\dot{x}_v + g_x(q) - B\left(\dot{\hat{x}} - \dot{x}_v\right) - Ge\end{aligned} \tag{10}$$

where $\dot{\hat{x}} = J(q)\hat{y}$ is the observed end-effector Cartesian velocity and the Cartesian position tracking error is given by $e = x - x_v$ where $x_v(t)$ is the virtual end-effector pose trajectory. The proportional and derivative gain matrices are G and B respectively. The controller's error dynamics is found by substituting controller (10) into (4) and invoking Appendix B. The expression for the trajectory error dynamics becomes

$$\begin{aligned}H_x(q)\ddot{e} &= -C_x(q,\dot{q})\dot{e} - F_x\dot{e} - B\dot{e} - Ge \\ &- J^{-T}C(q,J^{-1}\dot{x}_v)J^{-1}\dot{\tilde{x}} + H_x(q)\dot{\tilde{J}}J^{-1}\dot{x}_v + B\dot{\tilde{x}}\end{aligned} \tag{11}$$

where $\dot{\tilde{J}} = \dot{J} - \dot{\hat{J}} = \dot{J}(q,y) - \dot{J}(q,\hat{y})$.

B. Stability

Theorem 1. $\dot{\tilde{x}}, \dot{e}, e \to 0$ as $t \to \infty$ as long as the initial conditions for the state vector $\xi^T = \begin{bmatrix}\dot{e}^T & e^T & \dot{\tilde{x}}^T\end{bmatrix}$ satisfy

$$\Omega = \left\{\xi(0) : \|\xi(0)\| < \frac{1}{m_c}\sqrt{\frac{p_l}{2p_u}}\left[\underline{\sigma} + m_f - \frac{(k_b + m_x + m_c m_d)^2}{4(k_b + m_f)} - m_c m_d\right]\right\}$$

where gains K and B are designed such that $k_b > -m_f$ and $\underline{\sigma} > -m_f + (k_b + m_x + m_c m_d)^2/4(k_b + m_f) + m_c m_d$ where $\underline{\sigma} = \lambda_{\min}(J^{-T}KH(q)J^{-1} + J^{-T}H(q)KJ^{-1})/2$ and $B = k_b I$.

Proof. Consider the candidate Lyapunov function

$$v(t) = \frac{1}{2}\xi(t)^T P(q(t))\xi(t) \tag{12}$$

where $\xi^T = \begin{bmatrix}\dot{e}^T & e^T & \dot{\tilde{x}}^T\end{bmatrix}$ and $P(q) = \mathrm{diag}(H_x(q), G, H_x(q))$ with $G = G^T > 0$. Then (12) satisfies

$$\frac{1}{2}p_l\|\xi(t)\|^2 \le v(t) \le \frac{1}{2}p_u\|\xi(t)\|^2 \tag{13}$$

where $p_l = \lambda_{\min}(P(q))$ and $p_u = \lambda_{\max}(P(q))$. The derivative of (13) along all trajectories of $\xi(t)$ is given by

$$\dot{v} = \dot{e}^T\left(H_x(q)\ddot{e} + \frac{1}{2}\dot{H}_x(q)\dot{e} + Ge\right) + \dot{\tilde{x}}^T\left(H_x(q)\ddot{\tilde{x}} + \frac{1}{2}\dot{H}_x(q)\dot{\tilde{x}}\right) \tag{14}$$

Substituting observer and controller error dynamics (8) and (11) into (14) while using property 4 yields

$$\begin{aligned}\dot{v} = &-\dot{e}^T\left(F_x + B\right)\dot{e} - \dot{\tilde{x}}^T\left(F_x + J^{-T}H(q)KJ^{-1}\right)\dot{\tilde{x}} \\ &+\dot{e}^T B\dot{\tilde{x}} + \dot{e}^T H_x \dot{\tilde{J}} J^{-1}\dot{x}_v - \dot{e}^T J^{-T} C\left(q, J^{-1}\dot{x}_v\right)J^{-1}\dot{\tilde{x}} \\ &-\dot{\tilde{x}} J^{-T} C\left(q, J^{-1}\left(\dot{e} - \dot{\tilde{x}} + \dot{x}_v\right)\right)J^{-1}\dot{\tilde{x}}\end{aligned} \tag{15}$$

With the aid of property 2 and $\left\|\dot{\tilde{J}}\right\| = \left\|\dot{J}(q,y) - \dot{J}(q,\hat{y})\right\| = \left\|\dot{J}(q,\tilde{y})\right\| = \left\|\dot{J}\left(q, J^{-1}\dot{\tilde{x}}\right)\right\| \le m_2\left\|\dot{\tilde{x}}\right\|$ we can write (15) as

$$\begin{aligned}\dot{v} \le &-\left[k_b + m_f\right]\|\dot{e}\|^2 - \left[\underline{\sigma} + m_f - m_c m_d - m_c\left(\left\|\dot{\tilde{x}}\right\| + \|\dot{e}\|\right)\right]\left\|\dot{\tilde{x}}\right\|^2 \\ &+\left[k_b + m_x + m_c m_d\right]\|\dot{e}\|\left\|\dot{\tilde{x}}\right\|\end{aligned} \tag{16}$$

where $B = k_b I$, $\underline{\sigma} = \lambda_{\min}\left(J^{-T}KH(q)J^{-1} + J^{-T}H(q)KJ^{-1}\right)/2$, $m_f = \lambda_{\min}(F_x)$, $\|\dot{x}_v\| \le m_d$ and $m_x \ge \|H_x(q)\|\|J^{-1}\|\|\dot{x}_v\|$. Equation (16) can then be rewritten to obtain

$$\dot{v}(t) \le -\begin{bmatrix}\|\dot{e}\| \\ \left\|\dot{\tilde{x}}\right\|\end{bmatrix}^T \begin{bmatrix} k_b + m_f & -\frac{1}{2}\left(k_b + m_x + m_c m_d\right) \\ -\frac{1}{2}\left(k_b + m_x + m_c m_d\right) & \underline{\sigma} + m_f - m_c m_d - m_c\left(\left\|\dot{\tilde{x}}\right\| + \|\dot{e}\|\right)\end{bmatrix}\begin{bmatrix}\|\dot{e}\| \\ \left\|\dot{\tilde{x}}\right\|\end{bmatrix} \tag{17}$$

From (17) it can be deduced that if at $t = 0$ we have

$$k_b > -m_f \tag{18}$$

and

$$\underline{\sigma} > \frac{\left(k_b + m_x + m_c m_d\right)^2}{4\left(k_b + m_f\right)} - m_f + m_c m_d + m_c\left(\left\|\dot{\tilde{x}}(0)\right\| + \|\dot{e}(0)\|\right) \tag{19}$$

then $\dot{v}(0) < 0$ can be guaranteed. Furthermore, since $\sqrt{2}\|\xi(0)\| \ge \|\dot{e}(0)\| + \|e(0)\| + \left\|\dot{\tilde{x}}(0)\right\|$, it is evident that (19) holds if

$$\underline{\sigma} > \frac{\left(k_b + m_x + m_c m_d\right)^2}{4\left(k_b + m_f\right)} - m_f + m_c m_d + m_c\sqrt{2}\|\xi(0)\| \tag{20}$$

is satisfied. Then, (20) certainly holds if

$$\underline{\sigma} > \frac{\left(k_b + m_x + m_c m_d\right)^2}{4\left(k_b + m_f\right)} - m_f + m_c m_d + m_c\sqrt{\frac{2p_u}{p_l}}\|\xi(0)\| \tag{21}$$

is satisfied. So, if (21) is satisfied, then $\exists\, t < \delta$ for which $\dot{v}(t) < 0$. This implies that $v(t) < v(0)$ for $t < \delta$. As a consequence (13) tells us that $\|\xi(t)\| \le \sqrt{p_u/p_l}\|\xi(0)\|$ for $t < \delta$ from which we obtain

$$\|\dot{e}(t)\| + \left\|\dot{\tilde{x}}(t)\right\| \le \sqrt{\frac{p_u}{p_l}}\|\xi(0)\| \le 2\sqrt{\frac{p_u}{p_l}}\|\xi(0)\| \tag{22}$$

for $t < \delta$. As t goes on, it can be inferred from (17) that $\dot{v}(t) < 0$ as long as (18) and

$$\underline{\sigma} > \frac{\left(k_b + m_x + m_c m_d\right)^2}{4\left(k_b + m_f\right)} - m_f + m_c m_d + m_c\left(\|\dot{e}(t)\| + \left\|\dot{\tilde{x}}(t)\right\|\right) \tag{23}$$

hold. But (23) is satisfied by virtue of (21) and (22). Therefore, we have

$$\dot{v}(t) \le -\beta\left\|\begin{bmatrix}\|\dot{e}(t)\| \\ \left\|\dot{\tilde{x}}(t)\right\|\end{bmatrix}\right\|^2 \quad , \qquad \forall t \ge 0 \tag{24}$$

where $\beta > 0$. The region of stability is obtained by rewriting equations (21) for $\|\xi(0)\|$ explicitly, i.e.

$$\|\xi(0)\| < \frac{1}{m_c}\sqrt{\frac{p_l}{2p_u}}\left(\underline{\sigma} + m_f - \frac{\left(k_b + m_x + m_c m_d\right)}{4\left(k_b + m_f\right)} - m_c m_d\right) \tag{25}$$

Regarding stability, we note from (13) and (24) that $\dot{e}$, e, $\dot{\tilde{x}} \in L_\infty$ as long as initial conditions are satisfied by (25). Then we also have $\ddot{e}$, $\ddot{\tilde{x}} \in L_\infty$ by virtue of (8) and (11). Integration and reordering of (24) yields

$$\int_0^\infty \left\|\begin{bmatrix}\|\dot{e}(t)\| \\ \left\|\dot{\tilde{x}}(t)\right\|\end{bmatrix}\right\|^2 dt = \frac{1}{\beta}\left(v(0) - v(\infty)\right) < \infty$$

which implies $\dot{e}$, $\dot{\tilde{x}} \in L_2$. We can now apply Barbalat's Lemma to conclude that $\dot{e} \to 0$ as $t \to \infty$. Similarly $\dot{\tilde{x}} \to 0$ as $t \to \infty$. It is left to show the convergence of the position tracking error e. This is done by invoking Lasalle's theorem, consider (11); here we note that the largest invariant set is $e = 0$ since $\dot{e} \to 0$ and $\dot{\tilde{x}} \to 0$ as $t \to \infty$.

5. SIMULATION RESULTS

The manipulator considered for simulation of the observer plus impedance controller was a three degree of freedom planar manipulator based on a PUMA-560 subset. In particular, the second link of the PUMA-560 was chosen to be our first link, the third and fourth links of the PUMA-560 were chosen as a group to be our second link and the fifth and sixth PUMA links with force sensor and end-effector were chosen as a group to be our third link. The kinematic and dynamic parameters of the manipulator considered here were obtained from [9]. The dynamic equation based on (1) for our three degree of freedom manipulator is given below. The inertia matrix is defined by

$$\begin{aligned}H_{11} &= I_{m1} + I_{zz1} + I_{zz2} + I_{zz3} + m_1\left(r_{x1}^2 + r_{y1}^2\right) + m_2\left(a_1^2 + r_{x2}^2 + 2a_1 r_{x2} c_2\right) \\ &\quad + m_3\left(a_1^2 + a_2^2 + r_{x3}^2 + 2a_1 a_2 c_2 + 2a_1 r_{x3} c_{23} + 2a_2 r_{x3} c_3\right) \\ H_{12} &= I_{zz2} + I_{zz3} + m_2\left(r_{x2}^2 + a_1 r_{x2} c_2\right) \\ &\quad + m_3\left(a_2^2 + r_{x3}^2 + a_1 a_2 c_2 + a_1 r_{x3} c_{23} + 2a_2 r_{x3} c_3\right) \\ H_{13} &= I_{zz3} + m_3\left(r_{x3}^2 + a_1 r_{x3} c_{23} + a_2 r_{x3} c_3\right) \\ H_{22} &= I_{m1} + I_{zz2} + I_{zz3} + m_2 r_{x2}^2 + m_3\left(a_2^2 + r_{x3}^2 + 2a_2 r_{x3} c_3\right) \\ H_{23} &= I_{zz3} + m_3\left(r_{x3}^2 + a_2 r_{x3} c_3\right) \qquad H_{33} = I_{m1} + I_{zz3} + m_3 r_{x3}^2\end{aligned}$$

Symmetry defines the lower diagonal terms and a short form for trigonometric functions is given by $c_2 = \cos(q_2)$ and $c_{23} = \cos(q_2 + q_3)$. The matrix of Christoffel symbols is given by

$$
\begin{aligned}
C_{11} &= -m_2 a_1 r_{x2} \dot{q}_1 s_2 - m_3\left[a_1 a_2 \dot{q}_2 s_2 + a_1 r_{x3}(\dot{q}_1 + \dot{q}_2) s_{23} + a_2 r_{x3} \dot{q}_3 s_3\right] \\
C_{12} &= -m_2\left[a_1 r_{x2}(\dot{q}_1 + \dot{q}_2) s_2\right] \\
&\quad -m_3\left[a_1 a_2(\dot{q}_1 + \dot{q}_2) s_2 + a_1 r_{x3}(\dot{q}_1 + \dot{q}_2 + \dot{q}_3) s_{23} + a_2 r_{x3} \dot{q}_3 s_3\right] \\
C_{13} &= -m_3\left[a_1 r_{x3}(\dot{q}_1 + \dot{q}_2 + \dot{q}_3) s_{23} + a_2 r_{x3}(\dot{q}_1 + \dot{q}_2 + \dot{q}_3) s_3\right] \\
C_{21} &= m_2 a_1 r_{x2} \dot{q}_1 s_2 + m_3\left[a_1 a_2 \dot{q}_1 s_2 + a_1 r_{x3} \dot{q}_1 s_{23} - a_2 r_{x3} \dot{q}_3 s_3\right] \\
C_{22} &= -m_3 a_2 r_{x3} \dot{q}_3 s_3 \qquad C_{23} = -m_3 a_2 r_{x3}(\dot{q}_1 + \dot{q}_2 + \dot{q}_3) s_3 \\
C_{31} &= m_3\left(a_1 r_{x3} \dot{q}_1 s_{23} + a_2 r_{x3}(\dot{q}_1 + \dot{q}_2) s_3\right) \\
C_{32} &= m_3 a_2 r_{x3}(\dot{q}_1 + \dot{q}_2) s_3 \qquad C_{33} = 0
\end{aligned}
$$

The torques due to gravity are given by

$$
\begin{aligned}
g_1 &= m_1 g\left(r_{x1} c_1 - r_{y1} s_1\right) + m_2 g\left(a_1 c_1 + r_{x2} c_{12}\right) + m_3 g\left(a_1 c_1 + a_2 c_{12} + r_{x3} c_{123}\right) \\
g_2 &= m_2 g r_{x2} c_{12} + m_3 g\left(a_2 c_{12} + r_{x3} c_{123}\right) \qquad g_3 = m_3 g r_{x3} c_{123}
\end{aligned}
$$

and the matrix of damping coefficients is defined by $F = \mathrm{diag}(f_1, f_2, f_3)$. The Cartesian force/torque vector applied at the manipulator's end-effector is given by $F_{ext} = \left[f_x \quad f_y \quad n_z\right]$. The transpose of the Jacobian matrix is used to map the force/torque applied at the end-effector to torques applied at the joints. The Jacobian matrix is given by

$$
\begin{aligned}
J_{11} &= -\left(a_1 s_1 + a_2 s_{12} + a_3 s_{123}\right) \qquad J_{12} = -\left(a_2 s_{12} + a_3 s_{123}\right) \qquad J_{13} = -a_3 s_{123} \\
J_{21} &= a_1 c_1 + a_2 c_{12} + a_3 c_{123} \qquad J_{22} = a_2 c_{12} + a_3 c_{123} \qquad J_{23} = a_3 c_{123} \\
J_{31} &= 1 \qquad J_{32} = 1 \qquad J_{33} = 1
\end{aligned}
$$

The change of coordinates from joint space to Cartesian space requires the derivative of the Jacobian matrix. This is easily accomplished and the result will not be presented here. These relationships complete the description of the manipulator dynamic equation. Now, the particulars of the simulation will be described.

The kinematic parameters of the manipulator are its link lengths. Their values are $a_1 = 0.432$ m, $a_2 = 0.433$ m and $a_3 = 0.15$ m. The dynamic parameters consist of the link and motor inertias, link masses, link mass centers and dissipative coefficients. These are given as: $I_{zz1} = 0.539 \text{ kgm}^2$, $I_{zz2} = 0.212 \text{ kgm}^2$, $I_{zz3} = 0.006 \text{ kgm}^2$, $I_{m1} = 4.71 \text{ kgm}^2$, $I_{m2} = 0.830 \text{ kgm}^2$, $I_{m3} = 0.179 \text{ kgm}^2$, $m_1 = 17.4$ kg, $m_2 = 5.62$ kg, $m_3 = 1.00$ kg, $r_{x1} = 0.068$ m, $r_{y1} = 0.006$ m, $r_{x2} = 0.070$ m, $r_{x3} = -0.010$ m, $f_1 = 27.4$ kg/s, $f_2 = 4.54$ kg/s, $f_3 = 5.0$ kg/s where most have been obtained from [9].

The desired Cartesian end-effector trajectory specified consists of unconstrained and constrained motion parts. The unconstrained motion trajectory is described by the following truncated ellipse

$$
x_v(t) = \begin{bmatrix} 0.5 + 0.2\sin\left(2\pi f t - \pi/2\right) \text{ m} \\ 0.5\cos\left(2\pi f t - \pi/2\right) \text{ m} \\ 0.0 \text{ rad} \end{bmatrix}, \qquad x_{v1} < 0.65 \text{ m}
$$

where $f = 0.1$ Hz. Contact with the environment occurs when $x_{v1} \geq 0.65$ m and it is at contact that the desired or virtual trajectory switches to

$$
x_v(t) = \begin{bmatrix} 0.65196 \text{ m} \\ 0.5\cos\left(2\pi f t - \pi/2\right) \text{ m} \\ 0.0 \text{ rad} \end{bmatrix}, \qquad x_{v1} \geq 0.65 \text{ m}
$$

The virtual trajectory lies 0.00196 m inside the contact material and is depicted in Fig. 1a.

It is assuming that the material stiffness is 10^4 N/m so a depression of 0.00196 m creates a reaction equal to 19.6 N. The experiment was conducted using the observer given in (9) and the controller given in (10). The gains were as follows: for the observer $K = 50 I_{3x3}$ was used and for the controller $G = 1000 I_{3x3}$ and $B = 2\sqrt{1000} I_{3x3}$ were used. The update frequency was chosen as 400 Hz. The results of the simulation are shown in Figs. 1, 2 and 3.

Fig. 1a shows the desired Cartesian trajectory versus the actual Cartesian trajectory. The initial position of the end-effector was located at the coordinates $(p_x \quad p_y) = (0.3\,m \quad 0.0\,m)$. When the end-effector comes into contact with the environmental barrier at $x = 0.65$ m, there is a tracking overshoot which can be observed in more detail in Fig. 1b. Here the upper solid line represents the virtual trajectory and the dash line represents actual motion of the end-effector. The lower solid line represents the barrier. To observe the resulting contact force see Fig. 1d. To reduce the transient, the impedance of the manipulator could be increased; however, high impedance during contact motions can be highly destabilizing. The applied joint torques for the trajectory are given in Fig. 1c. The joint torques shown are well within the capability of the PUMA-560, see [9].

The observed versus actual Cartesian velocities are shown in Fig. 2. The actual x-velocity versus the observed x-velocity is shown in Fig. 2a The observer error for this direction is shown in Fig. 2c. The same graphics are shown for the y-direction in Figs. 2b and 2d. Note that the observer error tends to zero for both the x and y directions of motion.

The velocity tracking results are shown in Fig. 3. The desired x-velocity versus the actual x-velocity is displayed in Fig. 3a and the velocity tracking error for this motion direction is shown in Fig. 3c. Note that differences between the desired and actual trajectory velocities are due to initial controller startup and are also due to impact and separation of the end-effector to and from the contact surface.

Another way of implementing the impedance controller given in (10) is to use numerical differentiation for obtaining joint velocities. A Jacobian transformation was used to map the joint velocity estimate into end-effector Cartesian coordinates. The results of the simulation predict unstable bahaviour, see Fig. 4. The plot shows 0.25 sec of collected data. The oscillations noted in Fig. 4b continue to amplify and instability results. The results obtained here imply severe velocity maneuvers which could not be tolerated.

6. CONCLUSION

A reduced-order velocity observer plus impedance controller has been developed for constrained manipulator control. The observer plus impedance controller produces locally asymptotically stable observer, position, velocity and force tracking errors. The observer-controller was simulated for a three degree of freedom planar manipulator. The manipulator was made to track an elliptical end-effector trajectory truncated by a contact surface. During both unconstrained and constrained portions of the trajectory the observer plus impedance controller provided asymptotically stable behaviour. This was accomplished without the need for velocity measurement. A simulation was also performed where numerical differentiation was used to obtain a velocity for use in an impedance controller. The simulation predicted unstable manipulator behaviour.

REFERENCES

[1] N. Hogan, "Impedance control: an approach to manipulation: Part I - Theory," *Transactions of ASME, Journal of Dynamic Systems, Measurement and Control*, vol. 107, pp. 1-7, 1985.

[2] N. Hogan, "Impedance control: an appraoch to manipulation: Part II - Implementation," *Transactions of ASME, Journal of Dynamic Systems, Measurement and Control*, vol. 107, pp. 8-16, 1985.

[3] N. Hogan, "Impedance control: an approach to manipulation: part III - Applications," *Transactions of ASME, Journal of Dynamic Systems, Measurement and Control*, vol. 107, pp. 17-24, 1985.

[4] M.H. Raibert and J.J. Craig, "Hybrid Position/Force Control of Manipulators," *Journal of Dynamic Systems, Measurement and Control*, vol. 102, pp. 126-133, 1981.

[5] C.C. de Wit, K.J. Astom, and N. Fixot, "Computed torque control via a nonlinear observer," *International Journal of Adaptive Control and Signal Processing*, vol. 4, pp. 443-452, 1990.

[6] S. Nicosia and P. Tomei, "Robot control by using only position measurements," *IEEE Transaction on Automatic Control*, vol. 35, pp. 1058-1061, 1990.

[7] M. Erlic and W.S. Lu, "Manipulator control with and exponentially stable velocity observer," in *Proc. The American Control Conference*, 1992, pp. 1241-42.

[8] M.W. Spong and M. Vidyasagar, *Robot Dynamics and Control*, ,New York, NY: John Wiley & Sons, , 1989.

[9] B. Armstrong, O. Khatib, and J. Burdick, "The explicit dynamic and inertial parameters of the PUMA 560 arm," in *Proc. IEEE International Conference on Robotics and Automation*, 1986, pp. 510-518.

APPENDIX A

Observer Error Equation

Combine the expression for the observer (6) and the manipulator dynamic equation (5) to give the following

$$H(q)\dot{y} + C(q,y)y + Fy = H(q)\dot{\hat{y}} + C(q,\hat{y})\hat{y} + F\hat{y} - H(q)K\tilde{y} \tag{A1}$$

where $\tilde{y} = y - \hat{y}$. Some reorganization of (A1) yields

$$H(q)\dot{\tilde{y}} + C(q,y)y - C(q,\hat{y})\hat{y} + F\tilde{y} + H(q)K\tilde{y} = 0 \tag{A2}$$

but $C(q,y)y - C(q,\hat{y})\hat{y} = C(q,y)\tilde{y} + C(q,\hat{y})\tilde{y}$ so (A2) becomes

$$H(q)\dot{\tilde{y}} = -C(q,y)\tilde{y} - C(q,\hat{y})\tilde{y} - F\tilde{y} - H(q)K\tilde{y} \tag{A3}$$

Now, using the relationships given in (2) and (3), we apply the change of coordinates $\tilde{y} = J^{-1}\dot{\tilde{x}}$ and $\dot{\tilde{y}} = J^{-1}\left[\ddot{\tilde{x}} - \dot{J}J^{-1}\dot{\tilde{x}}\right]$ to equation (A3) to yield

$$H(q)J^{-1}\left[\ddot{\tilde{x}} - \dot{J}J^{-1}\dot{\tilde{x}}\right] = -C(q,y)J^{-1}\dot{\tilde{x}} - C(q,\hat{y})J^{-1}\dot{\tilde{x}} - FJ^{-1}\dot{\tilde{x}} - H(q)KJ^{-1}\dot{\tilde{x}}$$

rearranging and pre-multiplying this last expression by J^{-T} gives us

$$H_x(q)\ddot{\tilde{x}} = -C_x(q,\dot{q})\dot{\tilde{x}} - J^{-T}C(q,\hat{y})J^{-1}\dot{\tilde{x}} - F_x(q)\dot{\tilde{x}} - J^{-T}H(q)KJ^{-1}\dot{\tilde{x}}$$

This is the observer error equation expressed in the Cartesian coordinates.

APPENDIX B

Controller Error Equation

The controller error equation is obtained by substituting the controller given in (10) into (4). As a preliminary result we obtain

$$\begin{aligned} &H_x(q)\ddot{x} + C_x(q,y)\dot{x} + F_x\dot{x} \\ &\quad = H_x(q)\ddot{x}_v + C_x(q,\hat{y})\dot{x}_v + F_x\dot{x}_v - B\left(\dot{\hat{x}} - \dot{x}_v\right) - G\left(x - x_v\right) \end{aligned} \tag{B1}$$

Noting $\dot{\hat{x}} = \dot{x} - \dot{\tilde{x}}$ and reordering (B1) we get

$$H_x(q)\ddot{e} + C_x(q,y)\dot{x} - C_x(q,\hat{y})\dot{x}_v + F_x\dot{e} + B\dot{e} + Ge - B\dot{\tilde{x}} = 0 \tag{B2}$$

But

$$\begin{aligned} &C_x(q,y)\dot{x} - C_x(q,\hat{y})\dot{x}_v \\ &\quad = J^{-T}\left[C(q,y) - H(q)J^{-1}\dot{J}\right]J^{-1}\dot{x} \\ &\quad J^{-T}\left[C(q,\hat{y}) - H(q)J^{-1}\dot{\hat{J}}\right]J^{-1}\dot{x}_v \\ &\quad = J^{-T}\left[C(q,\dot{q}) - H(q)J^{-1}\dot{J}\right]J^{-1}\dot{e} \\ &\quad +J^{-T}\left[C(q,\dot{q}_v)J^{-1}\dot{\tilde{x}} - H(q)J^{-1}\left(\dot{\hat{J}} - \dot{J}\right)J^{-1}\dot{x}_v\right] \end{aligned}$$

from which we obtain

$$\begin{aligned} &C_x(q,y)\dot{x} - C_x(q,\hat{y})\dot{x}_v \\ &\quad = C_x(q,\dot{q})\dot{e} + J^{-T}C\left(q,J^{-1}\dot{x}_v\right)J^{-1}\dot{\tilde{x}} - H_x(q)\dot{\tilde{J}}J^{-1}\dot{x}_v \end{aligned} \tag{B3}$$

where $\dot{\tilde{J}} = \dot{J} - \dot{\hat{J}} = J(q,y) - J(q,\hat{y})$. Substituting (B3) into (B2) finalizes the expression for the controller error which is given by

$$\begin{aligned} &H_x(q)\ddot{e} + C_x(q,\dot{q})\dot{e} + J^{-T}C\left(q,J^{-1}\dot{x}_v\right)J^{-1}\dot{\tilde{x}} \\ &-H_x(q)\dot{\tilde{J}}J^{-1}\dot{x}_v + F_x\dot{e} + B\dot{e} + Ge - B\dot{\tilde{x}} = 0 \end{aligned}$$

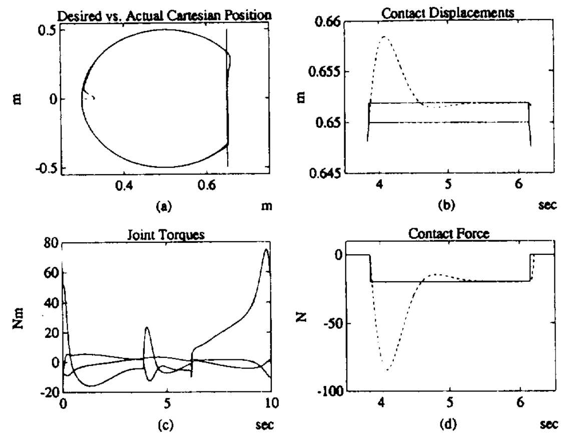

Fig. 1. Simulation results for position and force tracking (a) desired versus actual Cartesian position, (b) desired vs. actual displacements during contact, (c) applied joint torques, (d) desired vs. actual contact force.

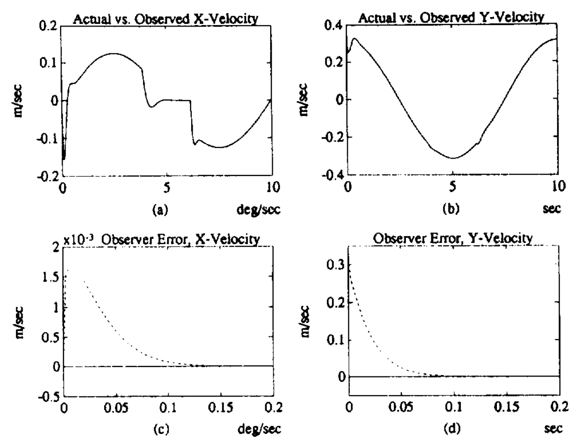

Fig. 2. Simulation results for the observer (a) actual velocity vs. observed velocity in x-direction, (b) actual velocity vs. observed velocity in y-direction, (c) observer error in x-direction (d) observer error in y-direction.

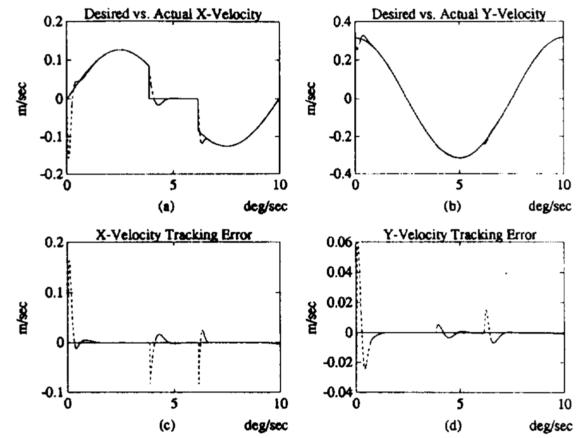

Fig. 3. Simulation results for the velocity tracking (a) desired velocity vs. actual velocity in x-direction, (b) desired velocity vs. actual velocity in y-direction, (c) velocity tracking error in x-direction (d) velocity tracking error in y-direction.

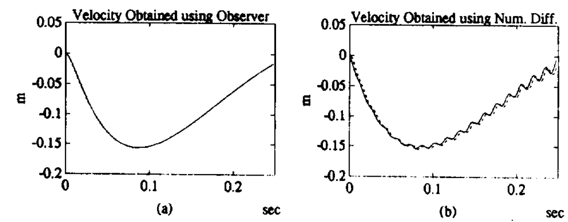

Fig. 4. Simulation results comparing end-effector velocity behaviour in the X-direction (a) actual vs. observed velocity, (b) actual velocity vs. velocity obtained with numerical differentiation.